

## Global Warming Patterns over the North Pacific: ENSO versus AO

Kazuki YAMAGUCHI

*R&D Center, Tokyo Electric Power Co., Yokohama, Japan*

and

Akira NODA

*Climate Research Department, Meteorological Research Institute, Tsukuba, Japan*

*(Manuscript received 31 May 2005, in final form 4 November 2005)*

### Abstract

The relationships between the natural variability and CO<sub>2</sub>-induced response over the Pacific region are investigated in terms of the spatial anomaly pattern of SST, sea level pressure and precipitation by a multi-model intercomparison analysis, based on the 18-model results contributing to the IPCC Fourth Assessment Report. The analysis indicates that the CO<sub>2</sub>-induced response pattern is related with the model natural variability modes, ENSO and AO. In the tropical Pacific, an ENSO-like global warming pattern is simulated by the majority of the models, with mostly El Niño-like change. In the Arctic region, an AO-like global warming pattern is simulated by many models, with the positive definite AO-phase change, if AO-like. It is suggested that the increase in meridional temperature gradient in the upper troposphere, and the lower stratosphere, provides a preferable condition for the positive AO-like change in the high latitudes by intensifying the subtropical jet, while the increase in the static stability provides a preferable condition for the El Niño-like change in the low latitudes, by reducing the large-scale ambient circulations. However, the sign of the mass (SLP) anomaly is incompatible over the North Pacific, between the positive AO-like change and the El Niño-like change. As a result, the present models cannot fully determine the relative importance between the mechanisms inducing the positive AO-like change and inducing the ENSO-like change, leading to scattering in global warming patterns in regional scales over the North Pacific.

### 1. Introduction

The projection of global warming can be regarded as a forcing-response problem in the presence of noise in the earth's climate system. In the context of the global warming issue, forcing is caused by the emission of greenhouse gases, and aerosols into the climate system due to human activities; the response is resultant

changes in the climatology, not only of the mean, but also of the variability in physical variables describing the climate system; the noise is usually called natural variability. If the noise is random, has no structure and can be assumed to be statistically independent of the response, we can identify the response as a signal of global warming rather easily. However, the situation is not simple for the case of the global warming, which is referred to as the attribution and detection issue (IPCC 2001). It is well known that the dominant modes of natural variability such as El Niño/Southern Oscillation (ENSO), and the Arctic Oscillation (AO), have distinct spatial structures. In addition, recent

---

Corresponding author: Kazuki Yamaguchi, R&D Center, Tokyo Electric Power Company, Inc., 4-1 Egasaki-cho, Tsurumi-ku, Yokohama, 230-8510, Japan.

E-mail: yamagu-k@rd.tepco.co.jp

© 2006, Meteorological Society of Japan

studies have shown that spatial response patterns to the greenhouse forcing resemble anomaly patterns of ENSO and AO as follows.

The El Niño/Southern Oscillation (ENSO) phenomenon is an oscillation of the sea surface temperature (SST), between a warm phase (El Niño) and a cool phase (La Niña) in the tropical Pacific, which is associated with an east-west sea level pressure anomaly (Southern Oscillation), and a variation of the Walker circulation. The ENSO is widely known as one of the most significant interannual and secular variations inherent in the large-scale climate system. How the ENSO itself changes in a warmer climate is naturally an important issue for the assessment (IPCC 2001). However, another interesting issue has arisen because some studies that employed coupled atmosphere-ocean general circulation models (AOGCMs) have shown that the CO<sub>2</sub>-induced warming response has a resemblance with the ENSO in the tropical Pacific (Knutson and Manabe 1995, 1998; Murphy and Mitchell 1995; Meehl and Washington 1997; Cane et al. 1997; Barnett 1999; Timmermann et al. 1999; Noda et al. 1999b; Cai and Whetton 2001a, 2001b). Although all these studies indicated ENSO-like responses to the increased CO<sub>2</sub> forcing, a discrepancy was observed among their polarities. Cane et al. (1997), and Noda et al. (1999b) predicted La Niña-like responses, while the others indicated El Niño-like responses. Noda et al. (1999b) performed doubling CO<sub>2</sub> ensemble experiments, with different initial conditions, by using an earlier version of the MRI AOGCM, the MRI-CGCM1, to confirm that the selection of the La Niña-like polarity is robust. However, when the same atmospheric part of the MRI-CGCM1 was coupled to a slab ocean model, Noda et al. (1999a) showed that an El Niño-like response appears referring to an ENSO-like natural variability mode in the Pacific SST reported by Kitoh et al. (1999b). Further, analyzing multi-model transient CO<sub>2</sub> runs, compiled in the IPCC Data Distribution Center for the Intergovernmental Panel on Climate Change (IPCC) Third Assessment Report (IPCC 2001), Noda (2000) showed that the response patterns resemble the spatial pattern of the leading mode of the model natural variability in the Pacific surface air temperature. Recently, however, using data submitted to the Coupled Model

Intercomparison Project (CMIP), Collins et al. (2005) made a multi-model comparison about the ENSO-like climate change for a narrower tropical Pacific zone, and concluded that no trends are found towards either mean El Niño-like or La Niña-like conditions.

In addition to the ENSO, the Arctic Oscillation (AO) and the Antarctic Oscillation (AAO) are also considered as interannual and secular natural variations. Found in the leading mode of the wintertime sea-level pressure (SLP) field in each hemisphere, the AO and AAO are observed as a seesaw of air mass, between high latitudes and the surrounding zonal ring in mid-latitudes. These are related to a fluctuation in the strength of the polar vortex (Baldwin et al. 1994; Perlwitz and Graf 1995; Cheng and Dunkerton 1995; Kitoh et al. 1996; Kodera et al. 1996; Thompson and Wallace 1998). The analyses based on observations, suggest that the AO recently exhibited a positive trend (Hurrell 1995; Thompson and Wallace 1998); it is considered that this may be a response to the increased CO<sub>2</sub> forcing. The model simulations indicated that the CO<sub>2</sub>-induced trend pattern in the Southern Hemisphere clearly projects on the AAO-like spatial pattern (Fyfe et al. 1999; Kushner et al. 2001; Cai et al. 2003), while the AO-like pattern is not so clear in the Northern Hemisphere, depending on the connection between the troposphere and the stratosphere (Shindell et al. 1999, 2001).

The studies mentioned above imply that spatial patterns of the CO<sub>2</sub>-induced trend are related to some extent with a similar mechanism working at the natural variability. However, it remains unclear as to what determines the selection of the mode and polarity of a natural variation pattern, on which a trend pattern projects. This study attempts to investigate the relationship between the natural variability and the CO<sub>2</sub>-induced response pattern by a systematic intercomparison, based on the state-of-the-art AOGCMs. For this purpose we use a new data set collected at the Program for Climate Model Diagnosis and Intercomparison (PCMDI), for the 4th Assessment Report of the IPCC. An outline of the models and experiments is described in section 2. The details of the simulated results, focusing on the ENSO-related variation in the Pacific region, and the AO-related variation in the Northern Hemi-

sphere, are given in section 3 and section 4, respectively. Finally, a discussion of the implications of these results, and the reasons for the diverse responses of the models, are presented in section 5.

## 2. The model and experiments

In the present study, we used the output of CMIP2-type run from each of the 18 models collected at the PCMDI (listed in Table 1); (a) a control run with a fixed concentration of CO<sub>2</sub> (pre-industrial or present-day) and (b) a transient CO<sub>2</sub> run, where CO<sub>2</sub> is increased from the control value at a compounded rate of 1% per year (to the CO<sub>2</sub> doubling, or quadrupling). The models and their simulations used for the present study are described in the PCMDI web site ([http://www-pcmdi.llnl.gov/ipcc/model\\_documentation/ipcc\\_model\\_documentation.php](http://www-pcmdi.llnl.gov/ipcc/model_documentation/ipcc_model_documentation.php)). For each model, the grid point data are

standardized onto the same 5 degrees in longitude by 4 degrees in latitude regular grid system, by the bi-linear interpolation method in order to compare the models characterized by different resolutions with each other. For ensemble experiments performed by FGOALS-g1.0 and MIROC3.2 (medres), only a single member (run-1) is used, because the differences between the ensemble members of a specific model are much less than those between the different models.

The natural variability patterns for the control runs are obtained by employing an empirical orthogonal function (EOF) analysis, to up to 200-year time series data. The CO<sub>2</sub>-induced linear trends are calculated by a least square fit from the trend difference between the 1% CO<sub>2</sub> run, and control run in years 11–70 or years 11–100, depending whether the 1% CO<sub>2</sub> run is performed up to the time of CO<sub>2</sub> doubling or

Table 1. Models used in this study.

Model	Originating Group(s)	Time length for EOF <sup>A</sup>	Time length for trend <sup>B</sup>
CCSM3	National Center for Atmospheric Research, USA	200 yrs	90 yrs
CGCM3.1(T47)	Canadian Centre for Climate Modelling & Analysis, Canada	200 yrs	90 yrs
CNRM-CM3	Météo-France/Centre National de Recherches Météorologiques, France	200 yrs	90 yrs
CSIRO-Mk3.0	CSIRO Atmospheric Research, Australia	200 yrs	60 yrs
ECHAM5/MPI-OM	Max Planck Institute for Meteorology, Germany	200 yrs	90 yrs
ECHO-G	MIUB/METRI of KMA/Model and Data group, Germany/Korea	161 yrs	90 yrs
FGOALS-g1.0	LASG/Institute of Atmospheric Physics, China	150 yrs	60 yrs
GFDL-CM2.0	US Dept. of Commerce/NOAA/Geophysical Fluid Dynamics Laboratory, USA	200 yrs	90 yrs
GFDL-CM2.1	US Dept. of Commerce/NOAA/Geophysical Fluid Dynamics Laboratory, USA	200 yrs	90 yrs
GISS-ER	NASA/Goddard Institute for Space Studies, USA	200 yrs	90 yrs
INM-CM3.0	Institute for Numerical Mathematics, Russia	200 yrs	90 yrs
IPSL-CM4	Institut Pierre Simon Laplace, France	200 yrs	90 yrs
MIROC3.2 (hires)	CCSR/NIES/Frontier Research Center for Global Change, Japan	100 yrs	60 yrs
MIROC3.2 (medres)	As above	200 yrs	90 yrs
MRI-CGCM2.3.2	Meteorological Research Institute, Japan	150 yrs	90 yrs
PCM	National Center for Atmospheric Research, USA	200 yrs	60 yrs
UKMO-HadCM3	Hadley Centre for Climate Prediction and Research/Met Office, UK	200 yrs	60 yrs
UKMO-HadGEM1	As above	200 yrs	60 yrs

<sup>A</sup>Time length used for the EOF analysis.

<sup>B</sup>Time length used to calculate the CO<sub>2</sub>-induced linear trend.

quadrupling, respectively. Here the first 10 years of the time series data are not used to avoid the cold start problem (IPCC 1996). Because the SLP data of the corresponding period are missing for ECHO-G control run, only the transient CO<sub>2</sub> run is used to compute the linear trend.

In order to study the ENSO-related variation of each model, the annual mean time series data of the SST from the control runs in the Pacific region (38°S–38°N, 120°E–60°W) are used first to compute the empirical orthogonal functions (EOFs). Here we take a latitudinal zone for analysis wider than that used by Collins et al. (2005), i.e., 10°S–10°N, because the ENSO has a coherent spatial structure over the whole Pacific region. The annual mean surface “skin” temperature (TS; i.e., SST for open ocean), sea level pressure (SLP), and precipitation are then regressed onto the normalized (i.e., unit standard deviation) time coefficients of the leading EOF (EOF1) of the SST to obtain the spatial patterns of natural variability.

A similar analysis was carried out for the AO-related variation of each model, except that the EOF analysis is based on the SLP over the Northern Hemisphere (north of 20°N), from the control runs. Here, the analysis is based on annual mean field, instead of wintertime, in order to be compared to the result from the Pacific region on the same basis. The annual mean SLP, TS, and precipitation are then regressed onto the normalized time coefficients of the leading EOF of the SLP, in order to obtain the spatial patterns of the natural variability.

### 3. ENSO-like natural variability and CO<sub>2</sub>-induced response

#### 3.1 Surface temperature

Figure 1 displays the spatial patterns, and time coefficients, of the first EOF of the observed annual mean SST anomalies (1903–2004) in the Pacific region (38°S–38°N, 120°E–60°W), from the NOAA Extended Reconstructed SST data set (Smith and Reynolds 2004), and associated regression patterns of annual mean SLP (1903–2000) from the Kaplan Extended SLP data set (Kaplan et al. 2000) provided by the NOAA-CIRES Climate Diagnostics Center. The spatial pattern of the leading EOF, exhibits a wedge-shaped anomaly in the equatorial Pacific, and anomalies of opposite polarity

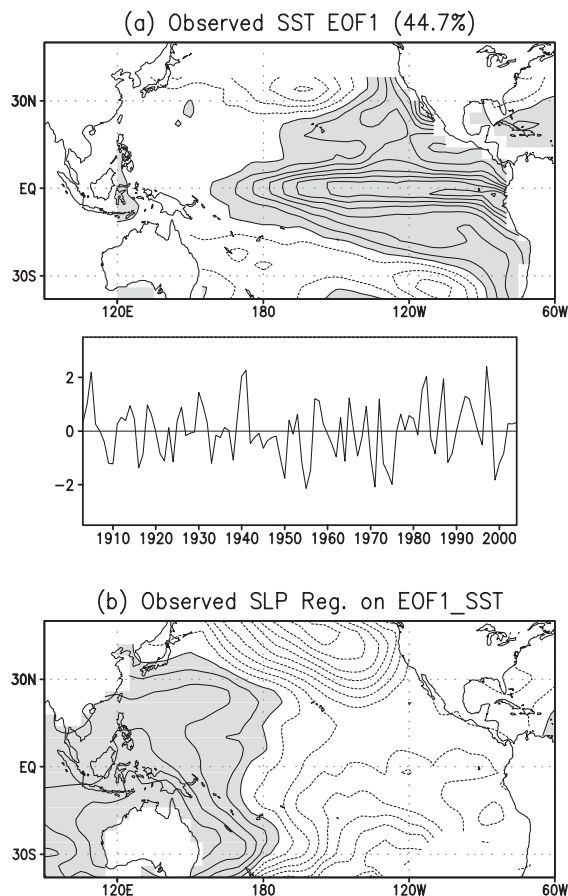


Fig. 1. (a) Spatial patterns and normalized time coefficients of the leading EOF for the observed annual mean SST anomalies over the Pacific (38°S–38°N, 120°E–60°W) for the period 1903–2004, and (b) associated regression pattern of annual mean SLP (1903–2000). The contribution of the EOF to the whole variance (%) is shown in the title. The contour interval is 0.1. Positive values are shaded.

in mid-latitudes in both hemispheres (Fig. 1a). This pattern is identified as the ENSO pattern, combined with a variation of the Walker circulation, and an east-west SLP anomaly (Fig. 1b).

Figure 2 shows CO<sub>2</sub>-induced linear trends (per 100 years), and the principal natural mode EOF1s simulated with the AOGCMs listed in Table 1. The 100-year linear trends are computed from the TS (1st and 3rd columns), and the natural variations are obtained in terms of the TS anomalies, regressed onto the normal-

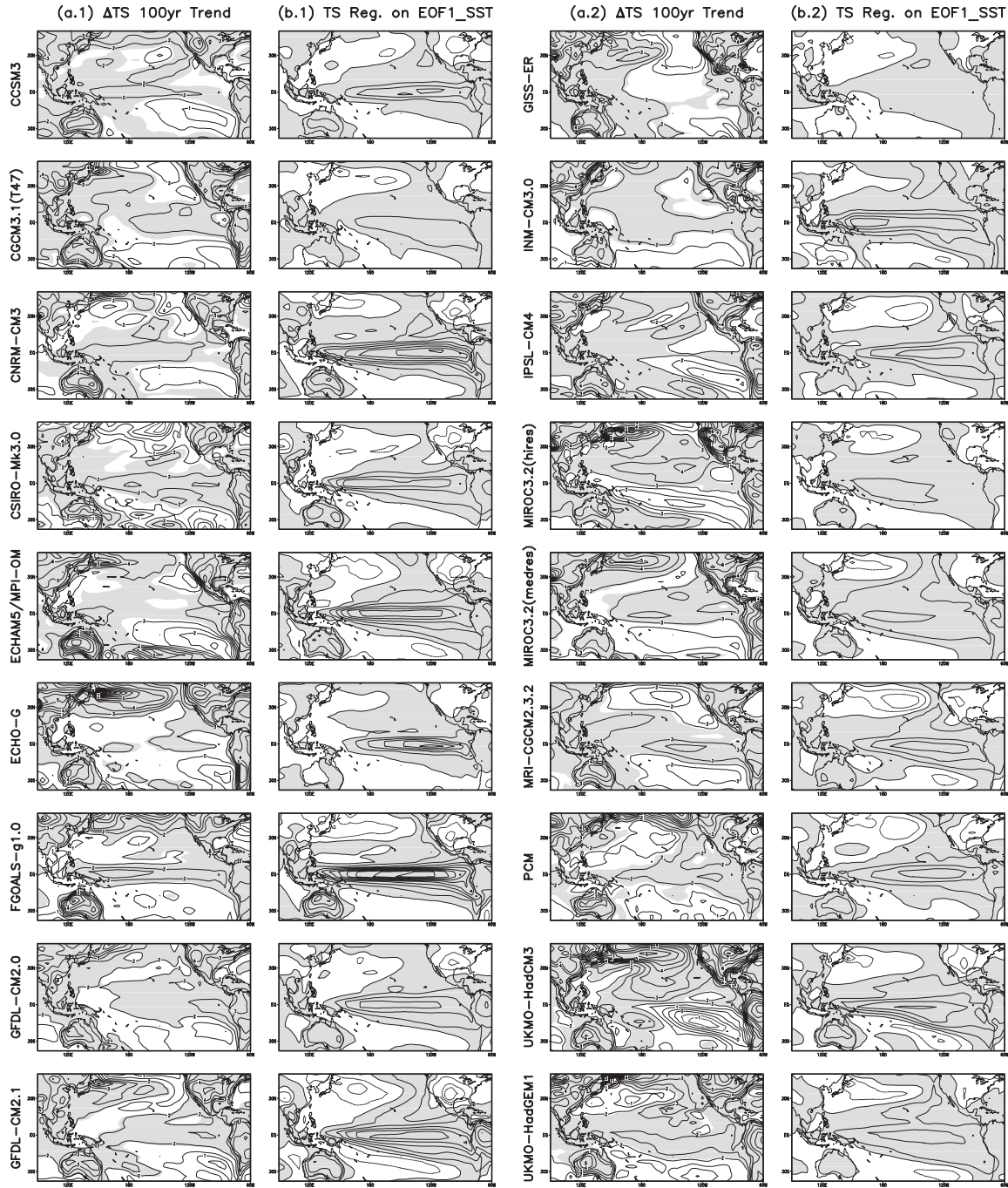


Fig. 2. (a) Simulated CO<sub>2</sub>-induced linear trend (transient minus control runs) per 100 years in the surface temperature (TS) (first and third columns). Model names are denoted on the left side of panels. The contour interval is 0.5 K. Dotted contours denote negative values. Shadings denote positive anomalies against the area averaged SST (38°S–38°N, 120°E–60°W) in the control run. (b) Simulated annual mean TS anomalies regressed onto the normalized time coefficients of the first mode of EOF for annual mean SST anomalies over the Pacific region (38°S–38°N, 120°E–60°W) in the control run (second and fourth columns). The contour interval is 0.2. Shadings denote positive values. All the maps are standardized to show the El Niño phase of the ENSO-like variability.

ized time coefficients of the leading mode (EOF1) of the SST (2nd and 4th columns). The simulated EOF1s are fairly similar among the models, and they capture the main features of the EOF1 of the observed SST (Fig. 1a), i.e., the ENSO pattern. Thus, all the EOF1 regression maps are standardized in Fig. 2 to exhibit the El Niño phase of the ENSO-like variability. The maximum variability tends to locate near the dateline for some models, although it is located more eastward in the observed SST field.

On the other hand, the CO<sub>2</sub>-induced trend patterns appear to be diverse among the models. For CGCM3.1 (T47), GFDL-CM2.0, GFDL-CM2.1, MRI-CGCM2.3.2 and PCM, the trend patterns have a maximum of warming in the equatorial eastern Pacific, while for CCSM3, CNRM-CM3, FGOALS-g1.0, GISS-ER, and UKMO-HadCM3, the trend patterns of the equatorial western Pacific exhibit a maximum warming. If we look at only the zonal temperature gradient along the equator (Meehl and Washington 1996), the models of the first and second groups could be classified as El Niño-like and La Niña-like, respectively. However, if we look at wider features over the Pacific, several models exhibit a similarity between the CO<sub>2</sub>-induced trend pattern and the EOF1 pattern. Therefore, it would be better to classify the trend pattern in terms of the polarity related to the model ENSO, including more wider zones.

In order to discuss the similarity more quantitatively, a pattern correlation analysis has been made as shown in Table 2. Here anomaly pattern correlation coefficients, between the trend and EOF1 in each model, are calculated from the SST data over the Pacific region for three latitudinal zones of different width, i.e., 10°S–10°N, 15°S–15°N and 38°S–38°N. We choose the correlation coefficients as a measure of “ENSONess” of the trend pattern. This result reveals that the dependency of the ENSONess on the zone width is different among the models. Some models (i.e., CCSM3.1 (T47), CNRM-CM3, GISS-ER, IPSL-CM4, MIROC3.2 (hires), and MRI-CGCM2.3.2) show very little dependency, but other models (except UKMO-HadGEM3) have a tendency to show lower ENSONess, in wider latitudinal zones. In the latter case, 10 models show absolute values of the correlation higher than 0.50 for the 10°S–

Table 2. Anomaly pattern correlation coefficients between the CO<sub>2</sub>-induced trend and the first EOF of the SST for three latitudinal zones with different width, i.e., 10°S–10°N, 15°S–15°N, and 38°S–38°N. Longitudinal range is 120°E–60°W, and land areas are masked.

Model	Correlation		
	±10°	±15°	±38°
CCSM3	0.36	0.33	0.32
CGCM3.1(T47)	0.43	0.29	0.03
CNRM-CM3	0.45	0.49	0.40
+ CSIRO-Mk3.0	0.81	0.82	0.59
ECHAM5/MPI-OM	0.22	0.21	0.08
(+) ECHO-G	0.65	0.44	0.02
+ FGOALS-g1.0	0.86	0.87	0.71
+ GFDL-CM2.0	0.65	0.60	0.45
+ GFDL-CM2.1	0.75	0.56	0.21
– GISS-ER	–0.61	–0.64	–0.65
INM-CM3.0	0.34	0.29	0.42
IPSL-CM4	–0.27	–0.25	–0.25
MIROC3.2 (hires)	–0.42	–0.43	–0.45
+ MIROC3.2 (medres)	0.51	0.42	0.18
+ MRI-CGCM2.3.2	0.71	0.68	0.69
+ PCM	0.85	0.84	0.68
– UKMO-HadCM3	–0.55	–0.54	–0.41
+ UKMO-HadGEM1	0.43	0.55	0.75
Mean absolute value	0.55	0.51	0.40

+ Model with a value of correlation higher than 0.50. Brackets mean a pattern conflict in the SLP field (see Section 3.2).

– Model with a value of correlation lower than –0.50.

10°N zone confined to equatorial Pacific, while the number of such models reduces down to 9 and 6 for the zones, 15°S–15°N and 38°S–38°N, respectively. Thus about a half of the models show an ENSO-like response in the low latitudes in the Pacific. Since the positive (negative) values of the correlation coefficients indicate the polarity, the same as the El Niño (La Niña) phase, the trend patterns of CSIRO-Mk3.0, ECHO-G, FGOALS-g1.0, GFDL-CM2.0, GFDL-CM2.1, MIROC3.2 (medres), MRI-CGCM2.3.2, PCM, and UKMO-HadGEM1 can be considered as El Niño-like, while those of GISS-ER and UKMO-HadCM3 can be regarded as La Niña-like.

Thus the results above suggest the existence

of a correlation between the natural variability and the trend pattern in each model, although its amplitude, and the choice of polarity, referring to the natural variability, depend on the models. However, it should be remarked that their similarities couldn't be applied to the trends over land areas, where strong warming trends are found regardless of the manner in which they project onto the natural variability patterns over the ocean area. In particular, anomalies over North America are observed as negative in the El Niño phase, but all the trend patterns exhibit a strong warming in the same region. This suggests that the warming over the land areas can be attributed to changes in the local heat balance, rather than those in the general circulation of the atmosphere.

### 3.2 Sea level pressure

Figure 3 compares the SLP aspect of the similarities shown in Fig. 2. The panels in the 1st and 3rd columns (Fig. 3a) represent CO<sub>2</sub>-induced trends, and those in the 2nd and 4th columns (Fig. 3b) represent the annual mean SLPs, regressed onto the time series of EOF1 of the SST. All the spatial patterns of EOF1, which are standardized to represent the El Niño phase, possess negative anomalies in the eastern equatorial Pacific, and positive anomalies in the Australian–Indonesian regions. These simulated patterns, capturing the main features of the observed pattern (Fig. 1b), are identified as the Southern Oscillation pattern. This characteristic pattern indicates that when the waters of the eastern Pacific are abnormally warm (an El Niño event), the SLP drops in the eastern Pacific, and rises in the western Pacific, which results in a reduction in the pressure gradient along the equator, thereby weakening the Walker circulation.

The 8 models which show El Niño-like SST trend patterns, namely, CSIRO-Mk3.0, FGOALS-g1.0, GFDL-CM2.0, GFDL-CM2.1, MIROC3.2 (medres), MRI-CGCM2.3.2, PCM, and UKMO-HadGEM1, also exhibit El Niño-like SLP trend patterns, i.e., the reduction in the pressure gradient along the equator. Moreover, GISS-ER and UKMO-HadCM3, show SLP trends consistent with the La Niña-like change. However, the similarities between the trend and EOF1 are not so clearly discernible in SLP as in SST, partly because the amplitude of the

SLP variability is generally smaller in low latitudes. In particular, ECHO-G has a large correlation, 0.65, based on the SST pattern for the zone 10°S–10°N, but it does not exhibit the El Niño-like SLP trend along the equator, so that we exclude the ECHO-G from the El Niño-like models in the discussion below. Another notable feature of the El Niño pattern found in the SLP field, is a strong anomaly in the middle North Pacific (see Fig. 1c for observation, and Fig. 2b for simulations). In terms of this feature, the SLP trends for 6 of the above-mentioned 8 models (except for GFDL-CM2.1 and MIROC3.2 (medres)) still can be considered as El Niño-like, even though the center of the negative anomaly tends to locate more northward than that in the EOF1 (El Niño) pattern. As for GFDL-CM2.1 and MIROC3.2 (medres), the SLP trend pattern conflicts with the El Niño pattern in mid-latitudes, because they have a strong positive anomaly in the middle North Pacific. These features found in the SLP trend, are consistent with the dependency of the SST spatial pattern correlation, on the zone width discussed in the previous section (see Table 2); when the latitudinal zone is extended to 38°S–38°N, the SST ENSOness for GFDL-CM2.1 and MIROC3.2 (medres) reduces to 0.21 and 0.18, respectively, while that for the other 6 models remains at high values.

The SLP results also confirm that there exists a relationship between the CO<sub>2</sub>-induced trend, and the natural variability in these models. It should also be noted that the EOF1 patterns of UKMO-HadCM3 and UKMO-HadGEM1 are similar to each other (Fig. 3a). Further, the trend patterns of them are also similar to each other, but have opposite polarity (Fig. 3b). This provides a typical example, indicating that a CO<sub>2</sub>-induced response pattern is closely related with the natural variability of a model; however, the selection of polarity is not fully deterministic among the models, which results in a significant scatter in the regional projection among the models.

### 3.3 Precipitation

Figure 4 compares the precipitation. The panels in the 1st and 3rd columns (Fig. 4a) represent CO<sub>2</sub>-induced trends, while those in the 2nd and 4th columns (Fig. 4b) represent the annual mean precipitation anomalies, re-

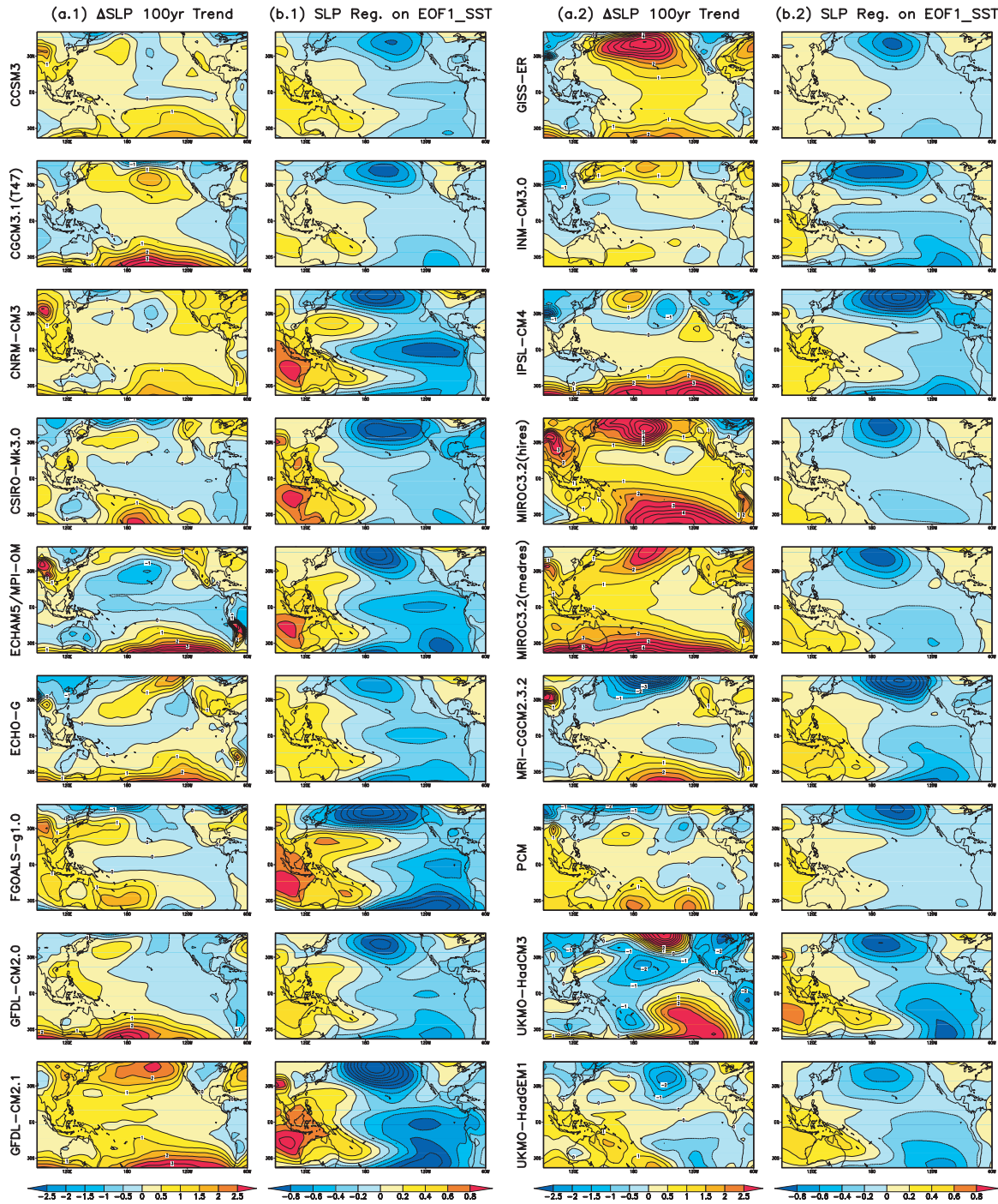


Fig. 3. Same as in Fig. 2, except for sea level pressure (SLP). (a) 100-year linear trends (contour interval: 0.5 hPa), and (b) the annual mean anomalies regressed onto the normalized time coefficients of the first and the second EOF of the SST (contour interval: 0.2).

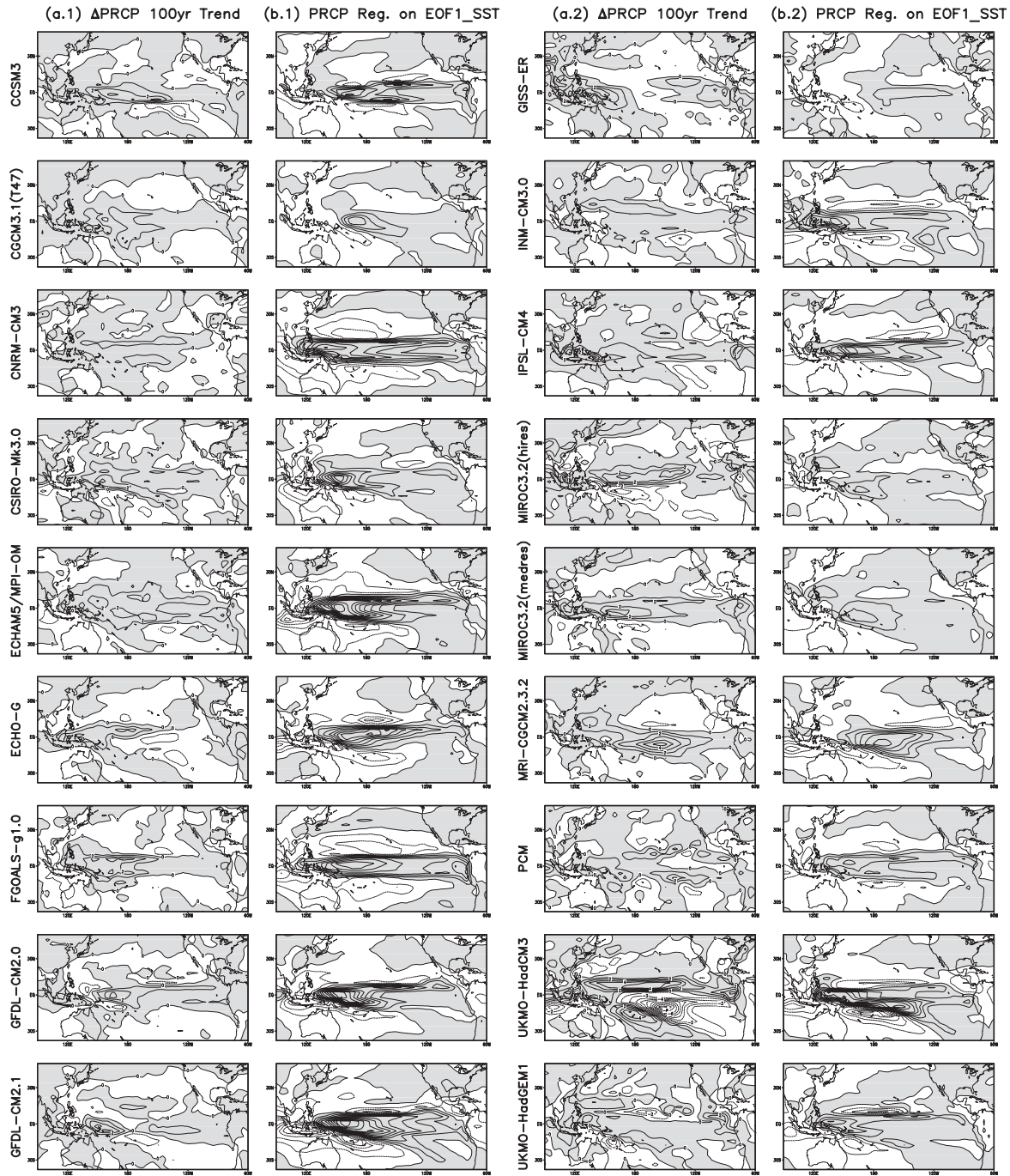


Fig. 4. Same as in Fig. 2, except for precipitation. (a) 100-year linear trends (contour interval: 1 mm/day), and (b) the annual mean anomalies regressed onto the normalized time coefficients of the first and the second EOF of the SST (contour interval: 0.3). Shadings denote positive values.

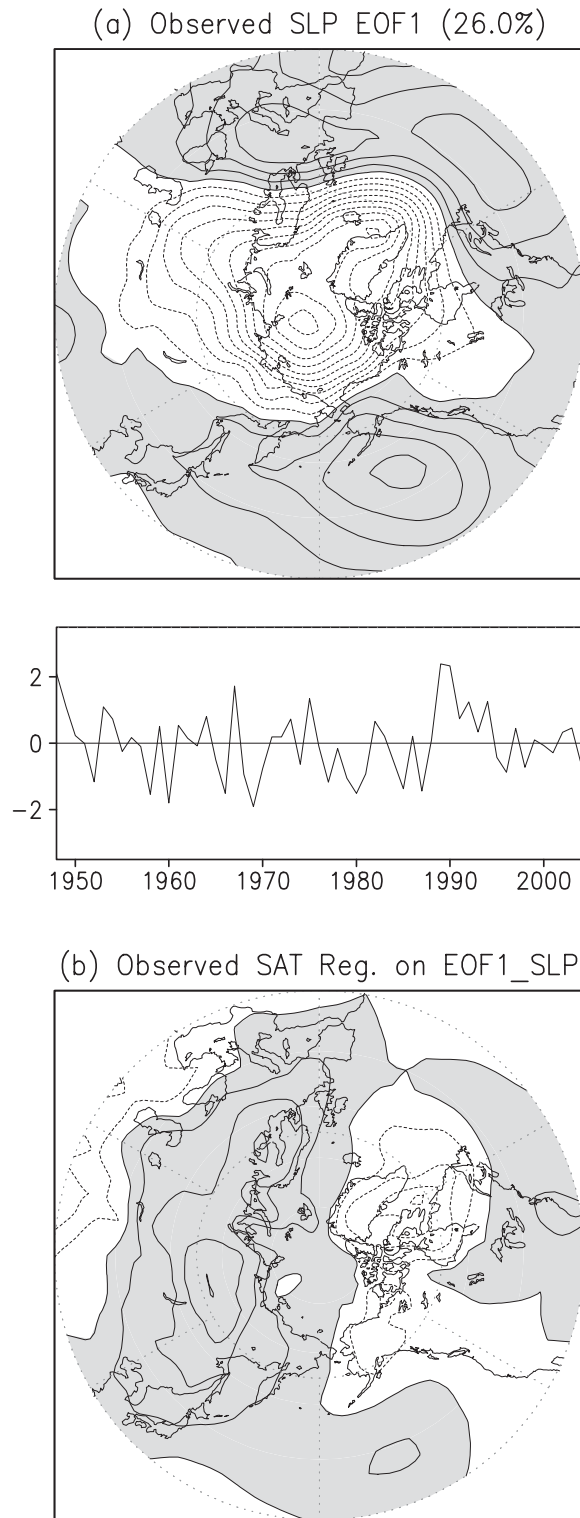


Fig. 5. (a) Spatial patterns and time coefficients of the leading EOF for the observed annual mean SLP anomalies

gressed onto the time series of the leading EOF of the SST. The polarity of the regression maps for EOF1, is selected to agree with the El Niño-like phase in Fig. 2.

The 8 models classified as El Niño-like in the previous sections, namely, CSIRO-Mk3.0, FGOALS-g1.0, GFDL-CM2.0, GFDL-CM2.1, MIROC3.2 (medres), MRI-CGCM2.3.2, PCM, and UKMO-HadGEM1, possess precipitation trend patterns that exhibit enhanced convective activity in the central Pacific. On the other hand, a La Niña-like trend in precipitation pattern is clearly seen in the western Pacific for GISS-ER and UKMO-HadCM3. Thus the relationship between the CO<sub>2</sub>-induced trend, and the natural variability, is consistent in the SST, SLP and precipitation fields for these models.

#### 4. The Arctic Oscillation and CO<sub>2</sub>-induced response

##### 4.1 Sea level pressure

In mid- and high latitudes, dominant natural variability modes have been mainly investigated referring to the pressure fields, such as SLP and 500-hPa height. Therefore we make here the same analysis as in the previous section, but begin with the SLP field in the Northern Hemisphere. Figure 5 shows a spatial pattern, and amplitude of the first EOF (EOF1), for the observed annual mean SLP anomaly field over a domain poleward of 20°N for the period 1948–2004 from the Trenberth's Northern Hemisphere Monthly Sea-Level Pressure Grids data (updated from Trenberth and Paolino 1980), provided by the NCAR Data Support Section, and associated regression patterns of annual mean surface air temperature (1948–2004), from the NCEP/NCAR Reanalysis data set (Kistler et al. 2001), provided by the NOAA-CIRES Climate Diagnostics Center. The EOF1 has a roughly zonally symmetric spatial pat-

field (north of 20°N, 1948–2004), and (b) associated regression pattern of annual mean surface air temperature. The spatial pattern is only shown for north of 30°N. The contribution of the EOF to the whole variance (%) is shown in the title. The contour interval is 0.2. Shadings denote positive values.

tern, with a negative SLP anomaly over the polar region, which is defined as the positive AO (Thompson and Wallace 1998).

Figure 6 compares linear trends (per 100 years) of the annual mean SLP, and the first EOF among the models. The standard deviation of the time series of the EOF coefficients is normalized, as in Fig. 2. The spatial patterns of EOF1 simulated by each model (Fig. 6b) are very similar to the observed pattern shown in Fig. 5a. In contrast, those of the CO<sub>2</sub>-induced trend show a larger scatter among the models. Nevertheless, some resemblances are found between the trend and the EOF1 pattern just as in Fig. 2 for the SST field. The trend patterns for CGCM3.1 (T47), ECHAM5/MPI-OM, GFDL-CM2.1, GISS-ER, INM-CM3.0, MIROC3.2 (hires), and MIROC3.2 (medres), possess negative anomalies in the polar region surrounded by a zonal ring of positive anomalies in the mid-latitudes, clearly indicating an AO-like change.

In order to quantitatively discuss these results, the anomaly pattern correlations, between the trend and the leading EOF, are calculated in Table 3 by using the SLP data over the whole domain, from 20°N to the North Pole. We choose the correlation coefficient as a measure of “AOness” of the trend pattern. The result confirms that the SLP trends show generally high AOness, with 11 models showing the correlation higher than 0.50. Thus nearly two thirds of the models show an AO-like response. In accordance with the negative anomaly in the polar region in the positive AO, every model shows a negative SLP trend in the polar region. Another feature that defines the positive AO pattern more strictly, is strong positive (anti-cyclonic) anomalies over the North Pacific and the North Atlantic (see Fig. 5a for observation, and Fig. 6b for simulations). However, some models fail to capture this feature either in the North Pacific (CSIRO-Mk3.0, FGOALS-g1.0, and UKMO-HadGEM1), or in the North Atlantic (ECHAM5/MPI-OM and MIROC3.2 (hires)). Actually, correlations of these models range from 0.52 to 0.62, which are relatively low among the eleven AO-like models.

#### 4.2 Surface temperature

As shown in Fig. 7b, the spatial patterns of the TS anomalies regressed onto the time se-

Table 3. Same as in Table 2 except for the SLP in the domain poleward of 20°N.

Model	Correlation
CCSM3	-0.31
+ CGCM3.1(T47)	0.69
CNRM-CM3	0.41
(+) CSIRO-Mk3.0	0.56
+ ECHAM5/MPI-OM	0.61
+ ECHO-G	0.73
(+) FGOALS-g1.0	0.52
GFDL-CM2.0	0.42
+ GFDL-CM2.1	0.79
+ GISS-ER	0.85
+ INM-CM3.0	0.76
IPSL-CM4	0.25
+ MIROC3.2 (hires)	0.59
+ MIROC3.2 (medres)	0.88
MRI-CGCM2.3.2	-0.22
PCM	0.42
UKMO-HadCM3	0.39
(+) UKMO-HadGEM1	0.62
Mean absolute value	0.56

+ Model with a value of correlation higher than 0.50. Brackets mean a pattern conflict in the North Pacific region.

ries of the EOF1 of the SLP, are fairly similar among the models, capturing the main features of the observed pattern (Fig. 5b). They exhibit a pattern with positive anomalies over the mid-North American Continent and Eurasia Continent, and negative anomalies over eastern Siberia, Alaska, northern Canada, Greenland and most of the Arctic basin. This pattern is a typical pattern associated with the positive AO (Thompson and Wallace 1998). On the other hand, the TS trend patterns, shown in Fig. 7a, possess strong positive anomalies around the Arctic basin, which are the typical effects of the sea/ice feedback forced by the CO<sub>2</sub>-induced warming (Manabe et al. 1991). Thus, the temperature anomaly patterns are clearly opposite between those associated with the positive AO, and those induced by the CO<sub>2</sub> radiative forcing in the high latitudes, except for Europe and west to middle Siberia. However, they possess a similar spatial structure in the mid-latitudes. In particular, in accordance with the anti-cyclonic SLP anomaly over the North Pacific, a strong positive TS trend is found over the

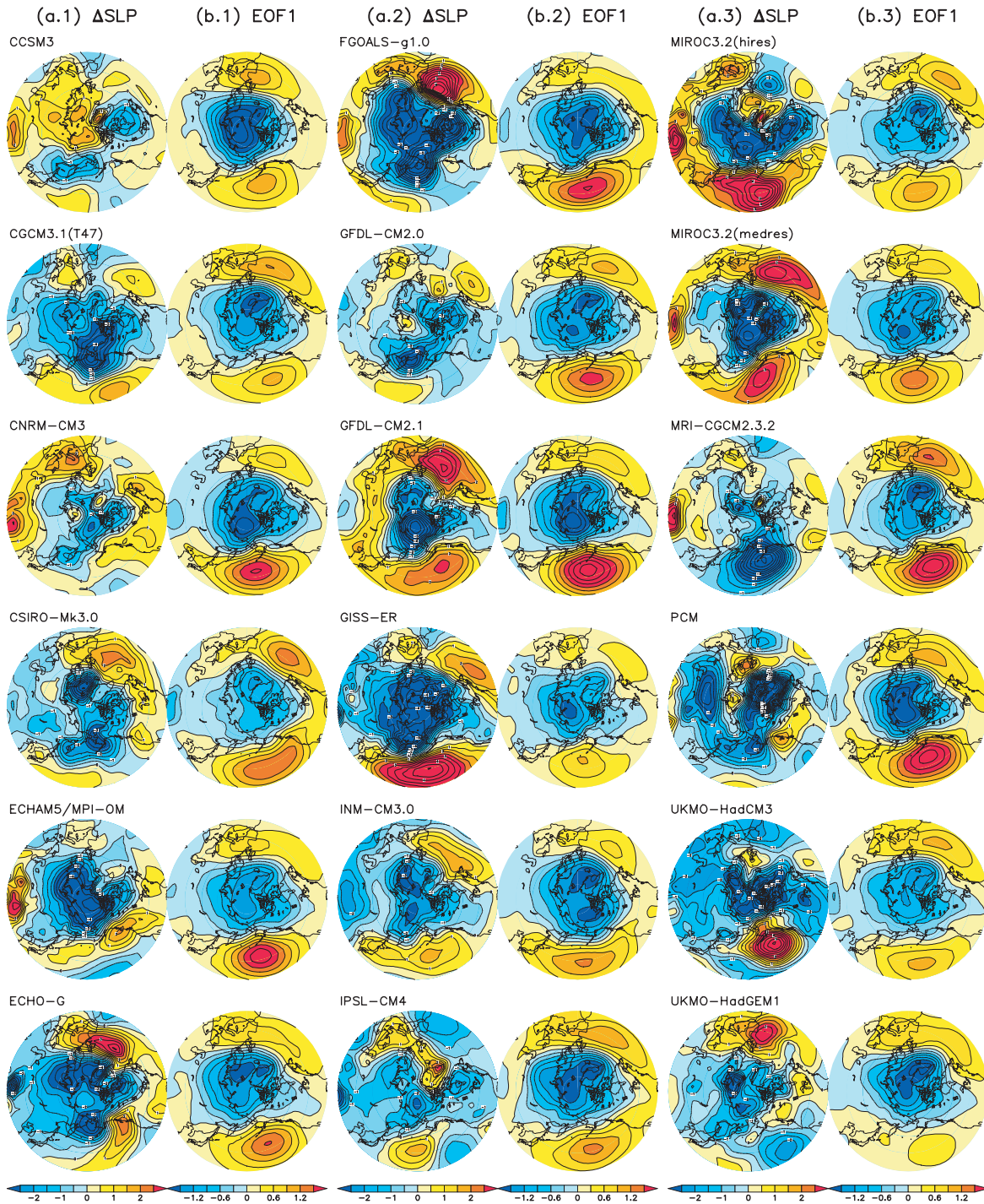


Fig. 6. (a) Simulated  $\text{CO}_2$ -induced linear trend (transient minus control runs) per 100 years in annual mean SLP with contour interval of 0.5 hPa (odd numbered columns). Model names are denoted on the top of panels. (b) The first mode of EOF for the annual mean SLP anomalies in the control run with contour interval of 0.3 (even numbered columns). The EOFs are calculated for the north of  $20^\circ\text{N}$ , however, it is shown only for the north of  $30^\circ\text{N}$ . All the maps are standardized to show the positive phase of the AO-like variability.

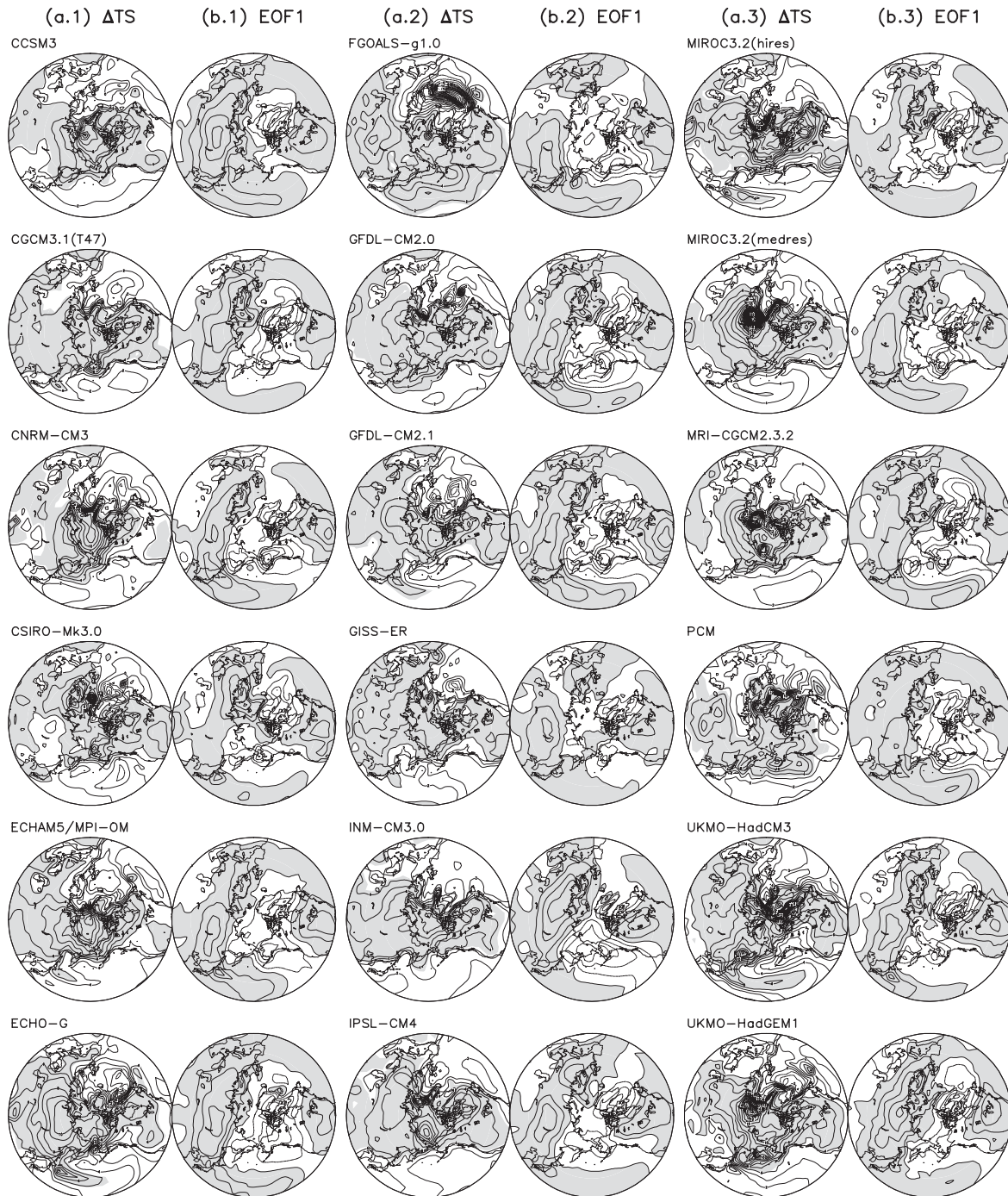


Fig. 7. Same as in Fig. 6, except for the TS. (a) 100-year linear trends (contour interval: 1 K). Dotted contours denote negative values. Shadings denote positive anomalies against the area average over 20°N–90°N. (b) The annual mean anomalies regressed onto the normalized time coefficients of EOF1 of SLP (contour interval: 0.2). Shadings denote positive values.

Kuroshio extension region for the 8 models that show AO-like SLP trend pattern, over the North Pacific (marked + in Table 3). A similar TS trend is evident for UKMO-HadCM3, because of a strong anticyclonic SLP trend in the North Pacific, although the AOness is low (0.39) for this model.

### 4.3 Precipitation

Figure 8 compares the spatial patterns between the trend, and the natural variability in the precipitation field. The natural mode is calculated by regressing the precipitation anomalies onto the time series of the leading EOF of the SLP. A rather uniform, positive anomaly in precipitation is found in high latitudes in both the trend and EOF1. It is not clear why the positive anomaly covers most of the Arctic basin for the positive AO, but it is known that precipitation increases generally in the high latitudes in a warmer climate, because the poleward water vapor transport increases due to the increase in water vapor, rather than in circulation (e.g., Wetherald and Manabe 2002). On the other hand, as is expected from the water vapor flux anomalies associated with the SLP anomalies, a zonal dipole pattern is found in the leading EOF over the North Pacific. Referring to the anomaly sign over the polar region, the opposite (same) anomaly sign is found in the central to eastern (western) North Pacific in the middle latitudes. A similar zonal dipole pattern is clearly found in the trend field for CGCM3.1 (T47), ECHO-G, GFDL-CM2.1, GISS-ER, MIROC3.2 (hires), and MIROC3.2 (medres), while for CNRM-CM3, GFDL-CM2.0, and MRI-CGCM2.3.2 in the opposite polarity. This may affect the precipitation trend in the regional scale between the models.

## 5. Discussion

### 5.1 Trend patterns classified referring to the AO and the ENSO

The results described above reveal that the natural variability pattern, and the CO<sub>2</sub>-induced trend pattern, are closely related for most of the AOGCMs. In previous studies, the El Niño-like trend and the AO-like trend, have been discussed independently, partly because the El Niño and the AO are rather independent natural variability, and defined by different variables, SST and SLP, and in different do-

main, tropical Pacific and mid- to high latitudes, respectively. However, since the El Niño is accompanied by the SLP variability, Southern Oscillation (SO), and affects the whole Pacific (see e.g., Figs. 1, 2b and 3b), the El Niño and the AO phenomena are overlapped in variable through SLP and in domain over the North Pacific. Therefore, if a trend pattern is related with the natural variability, we can expect that the pattern may be greatly affected in the common domain, i.e., the North Pacific.

In order to see the overlap effect, the ENSOness in Table 2, and the AOness in Table 3, are plotted as a scatter diagram in Fig. 9. As mentioned above, most models, except for CCSM3, CNRM-CM3 and IPSL-CM4 have some ENSOness and/or AOness in the trend patterns. There are several models that indicate high positive ENSOness (El Niño-like) and high AOness in Fig. 9. However, the high positive ENSOness for these models is achieved only for narrower zones. In specific, all the models with ENSOness higher than 0.5 for the 38°S–38°N zone show AOness lower than 0.65, while all the models with AOness higher than 0.65 show ENSOness lower than 0.5 for the 38°S–38°N zone. On the other hand, GISS-ER shows high AOness and robust, large negative ENSOness (La Niña-like). The reason is simple; the model with a high AOness trend should take a positive SLP (SST) anomaly in the North Pacific, but the model with a high positive ENSOness (El Niño-like) trend should take a negative SLP (SST) anomaly over the same region (see Figs. 3 and 6 for SLP, and Figs. 2 and 7 for SST). The latter aspect has been missed in previous studies, because the ENSO-like climate change has been analyzed mainly focusing on near the Pacific equator (Collins et al. 2005).

Thus many models seem to take an El Niño-like, and AO-like trend, but the relative tendency is different among the models, which causes a large scatter in SST, SLP and precipitation in the CO<sub>2</sub>-induced warmer climate.

### 5.2 El Niño-like change vs. AO-like change

Here we will discuss why many models tend to show an AO-like change trend and/or an ENSO-like trend in a warmer climate.

If we can assume that the main structure of the positive AO is related with the intensification and zonal symmetrization of the subtropi-



Fig. 8. Same as in Fig. 6, except for the precipitation. (a) 100-year linear trends (contour interval: 0.3 mm/day), and (b) the annual mean anomalies regressed onto the normalized time coefficients of EOF1 of SLP (contour interval: 0.05). Shadings denote positive values.

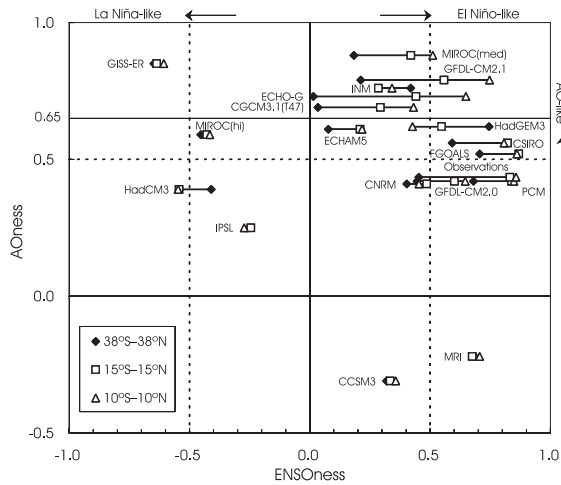


Fig. 9. Scatter diagram of “ENSONess” versus “AONess” for the simulated trend patterns. “ENSONess” and “AONess” are expressed in terms of the pattern correlation shown in Table 2 and Table 3, respectively. The “observations” is based on the historical observations shown in Figs. 1, 5 and 10.

cal westerly jet, we can expect that a CO<sub>2</sub>-induced forcing provides preferable conditions for the positive AO-like change as follows. Firstly, when the atmospheric concentration of the greenhouse gases are increased, the most notable difference in the temperature response, between the troposphere and the stratosphere is the fact that the troposphere becomes warmer, but the stratosphere becomes cooler, due to the difference in heat balance (Manabe and Wetherald 1967). On the other hand, since the height of the tropopause is higher in low latitudes than in high latitudes, the meridional temperature gradient increases along the mean tropopause level, between the equator and the pole, which leads to an intensification of the westerly jet. A similar mechanism works in the upper troposphere, because temperature increases larger in the upper troposphere, than at the surface in low latitudes in a warmer climate. This response is robust among the models, because the cumulus convections keep the lapse rate near the moist adiabatic lapse rate in low latitudes, and the moist adiabatic lapse rate decreases as temperature increases. Secondly, in a warmer climate a large surface

temperature increase occurs below the troughs of planetary waves in high latitudes (Noda 1996). Such a warming provides a preferable forcing for the jet to be more symmetric. Thus these basic mechanisms suggest that the climate system is forced to take a positive AO-like change in a warmer climate.

On the other hand, several mechanisms, inducing an El Niño-like change and those inducing a La Niña-like change, have been proposed. Knutson and Manabe (1995) showed that a general decrease in Walker circulation occurs due to increase in static stability in the troposphere in a warmer climate. They also attributed a damping of the east-west SST gradient, to the east-west differential in evaporative surface cooling (with greater evaporative cooling in the west than in the east), due to the temperature dependence of saturation mixing ratios. Meehl and Washington (1996) related it to the SST/convective clouds/solar radiation (negative) feedback (or thermostat effect), in the western Pacific. The damping of the east-west SST, brings the reduction of the Walker circulation. In contrast, Cane et al. (1997) argued that the enhanced longwave heating at the surface should be balanced by increasing a cold water advection and/or upwelling, which demands an intensification of the Walker circulation. Thus there seems to be little clues to determine whether the El Niño-like change or the La Niña like change is more possible in a warmer climate, as long as only the Walker circulation is concerned. However, the mechanism about the change in static stability (Knutson and Manabe 1995; see also Sugi et al. 2002, and Sugi and Yoshimura 2004) may give us an insight into the change in intensity of the Walker circulation, because such a mechanism is applicable to the Hadley circulation, and the Brewer-Dobson circulation as follows.

In the low latitudes, the main balance in the thermodynamic equation is:

$$\omega \frac{\partial \theta}{\partial p} \approx Q,$$

where  $\omega$  is the vertical velocity in the pressure  $p$  coordinate,  $\theta$  is the potential temperature,  $Q$  is the net heating and a zonal and sufficiently long-term average is taken over these variables. In a greenhouse gas, induced-warmer climate,  $\omega$ ,  $\theta$  and  $Q$  are changed to  $\omega + \Delta\omega$ ,  $\theta + \Delta\theta$  and

$Q + \Delta Q$  with  $|\Delta\omega/\omega|$ ,  $|\Delta\theta/\theta|$  and  $|\Delta Q/Q| \ll 1$  so that

$$\Delta\omega \frac{\partial\theta}{\partial p} + \omega \frac{\partial\Delta\theta}{\partial p} \approx \Delta Q.$$

Here  $\partial\Delta\theta/\partial p$  in the second term in the left hand side is regarded as the main source to induce the change in  $\omega$  and  $Q$ , because the main feature of the vertical temperature profile and its change is determined, by simple energy balance models such as a one-dimensional radiative-convective equilibrium model (Takata and Noda 1998), where  $\omega$  and  $Q$  vanish. Since the change  $\partial\Delta\theta/\partial p$  is a result of an adjustment process to reduce the net heating  $Q$ , we may assume that the dynamical response  $\Delta\omega$  dominates the net heating adjustment  $\Delta Q$ . Now that the maximum warming occurs in the upper troposphere, which means  $\partial\Delta\theta/\partial p < 0$  in the middle and lower troposphere, the balance in the right hand side demands that  $\Delta\omega$  should be positive, that is, the Hadley circulation weakens in the warmer climate. This suggests that the main circulations tend to weaken in the low latitudes, even though local circulations can intensify. The general weakening of the circulations also indicates that the heat balance proposed by Cane et al. (1997) cannot dominate throughout the low latitudes in general, because of weakening of the wind driven ocean circulations. Actually, Kitoh et al. (1999a) showed by analyzing a CMIP run with the MRI-CGCM1, which showed a La Niña-like response, that the Indian summer monsoon circulation weakens in a warmer climate although the water vapor transport is intensified. In addition, recently, Tanaka et al. (2005) showed that Hadley, Walker, and monsoon circulations are weakened in a warmer climate according to the ensemble mean of the IPCC 21<sup>st</sup> century model simulations. Further, if the same argument is applied to the stratospheric response, we can expect that the Brewer-Dobson circulation intensifies in a greenhouse gas abundant climate, because  $\partial\Delta\theta/\partial p > 0$  in the stratosphere (Manabe and Wetherald 1967). Actually, a consistent response is simulated by Rind et al. (2002), in that the residual circulation increases with the atmospheric CO<sub>2</sub> concentration doubled.

Thus the atmospheric feedback processes in the low latitudes provide a preferable condition for the El Niño-like change, suggesting that

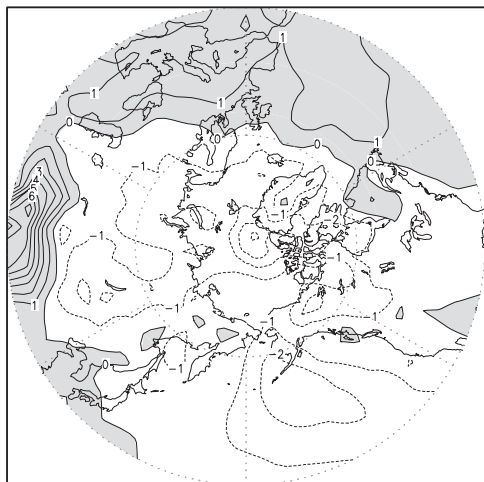
most of the present models prefer the positive ENSOness in Fig. 9.

There remains a possibility that the above mechanisms for the AO-like change, and the ENSO-like change are strongly coupled. However, as far as the natural variability is concerned, modeling and observational studies indicate at most a weak coupling between the ENSO and AO (Hamilton 1993; Baldwin and O'Sullivan 1995; Kitoh et al. 1996). Actually, while the ENSO related variability is strongly coupled with the SST variability, the AO-like variability can be simulated under a fixed SST condition (Yamazaki and Shinya 1999). The scatter shown in Fig. 9 indicates that the present models cannot fully determine the relative importance between the mechanism(s) inducing a positive AO-like change, and the mechanism(s) inducing an ENSO-like change. Then how can we determine the most likely response pattern for the future climate change? The observed trends may give us a hint. Figure 10a displays a linear trend map for the observed annual mean SLP anomalies over the northern hemisphere for the period 1948–2000 (updated from Trenberth and Paolino 1980). On the whole, it is similar to the positive phase of the AO; however, the negative anomalies over the North Pacific are notably dissimilar. On the other hand, for the Pacific region, the linear trends in the observed annual mean SST (NOAA Extended Reconstructed SST; Smith and Reynolds 2004), and SLP (Kaplan Extended SLP; Kaplan et al. 2000) field for this period, as shown in Figs. 10b and 10c, distinctly exhibit an El Niño-like structure, which is consistent with the decreasing SLP over the North Pacific. The ENSOness and the AOness for the observed historical trend is also shown in Fig. 9. Thus if the observed trends for the last fifty years are mainly attributable to the CO<sub>2</sub>-induced change, then the models that show high (positive) ENSOness/low AOness (see Fig. 9) would have a better performance than the other models.

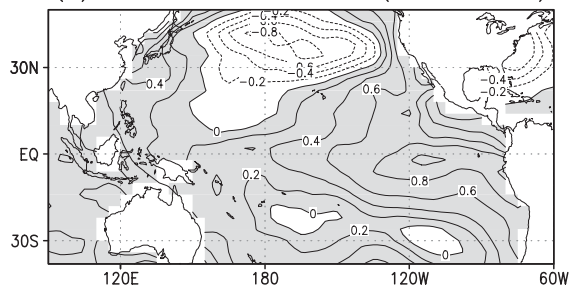
## 6. Concluding Remarks

The relationships between the natural variability, and CO<sub>2</sub>-induced response over the Pacific region, are investigated in terms of the spatial anomaly pattern of SST, sea level pressure and precipitation by a multi-model inter-

(a) observed SLP trend (1948–2000)



(b) observed SST trend (1943–2000)



(c) observed SLP trend (1943–2000)

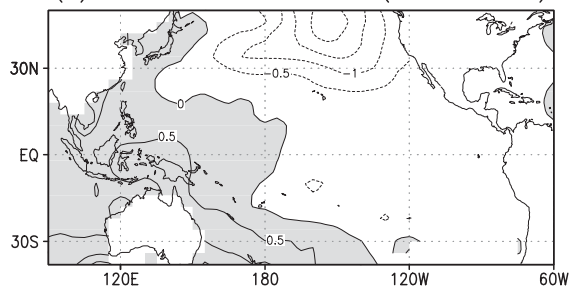


Fig. 10. (a) Linear trends for observed annual mean SLP anomalies (1948–2000) over the region north of 30°N. Contour interval is 1 hPa. (b) Linear trends for the observed annual mean SST anomalies (1943–2000) over the Pacific region. Contour interval is 0.3 K. (c) As in (b), for the SLP. Contour interval is 0.5 hPa. Shadings denote positive values.

comparison analysis, using the IPCC Data Archive at Lawrence Livermore National Laboratory.

All the models simulated well the leading modes of natural variability, such as ENSO and AO, and the spatial anomaly patterns for them are fairly similar among the models. Most of the models simulated CO<sub>2</sub>-induced response patterns, that suggest a resemblance with their model natural variability modes. However, the similarity among the response patterns is not so clear, compared to that among the natural variability patterns.

We have classified the response patterns referring to the main natural variability modes. In the tropical Pacific, a global warming pattern, with positive ENSOness, is simulated by many models. In the Arctic region, an AO-like global warming pattern, is simulated by many models, with the positive definite AO-phase change if AO-like.

We have discussed the mechanisms inducing the AO-like change, or the ENSO-like change. It is shown that a mechanism based on the change in the meridional temperature field can explain both the AO-like change and the ENSO-like change consistently. The change in meridional temperature gradient in the upper troposphere, and the lower stratosphere, provides a preferable condition for the positive AO-like change in the high latitudes by intensifying the subtropical jet, while the change in the static stability, provides a preferable condition for the El Niño-like change in the low latitudes, by reducing the existing main circulations. However, the sign of the mass (SLP) anomaly is incompatible over the North Pacific, between the positive AO-like change and the El Niño-like change. As a result, the current models are wandering to determine which change dominates a warmer climate over the North Pacific.

The mechanisms discussed in this paper may be different from that proposed by Palmer (1993, 1999), based on studies of nonlinear chaotic models, with preferred states or regimes. We have not made a systematic analysis for the probability density function (PDF) of El Niño and La Niña, but have not found evidence that the PDF of El Niño increases systematically in the model simulations showing the El Niño-like change. Since it is reported that several papers are submitted to investigate the

PDF change in a warmer climate, we will discuss this matter in a separate paper.

### Acknowledgments

We acknowledge the international modeling groups for providing their data for analysis, the Program for Climate Model Diagnosis and Intercomparison (PCMDI) for collecting and archiving the model data, the JSC/CLIVAR Working Group on Coupled Modeling (WGCM) and their Coupled Model Intercomparison Project (CMIP) and Climate Simulation Panel for organizing the model data analysis activity, and the IPCC WG1 TSU for technical support. The IPCC Data Archive at Lawrence Livermore National Laboratory is supported by the Office of Science, U.S. Department of Energy. This research has also been supported by the Japan Meteorological Agency's Climate Prediction Fund (Study on Prediction of Global Warming), and Joint Study between the MRI and the Tokyo Electric Power Co. Comments from the anonymous reviewers were valuable in improving the manuscript.

### References

- Baldwin, M.P., X. Cheng, and T.J. Dunkerton, 1994: Observed correlations between winter-mean tropospheric and stratospheric circulation anomalies. *Geophys. Res. Lett.*, **21**, 1141–1144.
- and D. O'Sullivan, 1995: Stratospheric effects of ENSO-related tropospheric circulation anomalies. *J. Climate*, **8**, 649–667.
- Barnett, T.P., 1999: Comparison of near surface air temperature variability in eleven coupled global climate models. *J. Climate*, **12**, 511–518.
- Cai, W. and P.H. Whetton, 2001a: Modes of SST variability and the fluctuation of global mean temperature. *Clim. Dyn.*, **17**, 889–901.
- and ———, 2001b: A time-varying greenhouse warming pattern and the tropical-extratropical circulation linkage in the Pacific Ocean. *J. Climate*, **14**, 3337–3355.
- , ———, and D.J. Karoly, 2003: The response of the Antarctic Oscillation to increasing and stabilized atmospheric CO<sub>2</sub>. *J. Climate*, **16**, 1525–1538.
- Cane, M.A., A.C. Clement, A. Kaplan, Y. Kushnir, R. Murtugudde, D. Pozdnyakov, R. Seager, and S.E. Zebiak, 1997: 20th century sea surface temperature trends. *Science*, **275**, 957–960.
- Cheng, X. and T.J. Dunkerton, 1995: Orthogonal rotation of spatial patterns derived from singular value decomposition analysis. *J. Climate*, **8**, 2631–2643.
- Collins, M., The CMIP Modeling Groups (BMRC (Australia), CCC (Canada), CCSR/NIES (Japan), CERFACS (France), CSIRO (Australia), MPI (Germany), GFDL (USA), GISS (USA), IAP (China), INM (Russia), LMD (France), MRI (Japan), NCAR (USA), NRL (USA), Hadley Centre (UK), and YNU (South Korea)), 2005: El Niño- or La Niña-like climate change? *Clim. Dyn.*, **24**, 89–104, DOI 10.1007/s00382-004-0478-x.
- Fyfe, J.C., G.J. Boer, and G.M. Flato, 1999: The Arctic and Antarctic Oscillations and their projected changes under global warming. *Geophys. Res. Lett.*, **26**, 1601–1604.
- Hamilton, K., 1993: An examination of observed Southern Oscillation effects in the Northern Hemisphere stratosphere. *J. Atmos. Sci.*, **50**, 3468–3473.
- Hurrell, J.W., 1995: Decadal trends in the North Atlantic Oscillation: Regional temperatures and precipitation. *Nature*, **269**, 676–679.
- IPCC, 1996: *Climate Change 1995: The Science of Climate Change. Contribution of Working Group I to the Second Assessment Report of the Intergovernmental Panel on Climate Change*. Cambridge University Press, Cambridge, United Kingdom, 572 pp.
- IPCC, 2001: *Climate Change 2001, The Scientific Basis. Contribution of Working Group I to the Third Assessment Report of the Intergovernmental Panel on Climate Change*. Cambridge University Press, Cambridge, United Kingdom, 881 pp.
- Kaplan, A., Y. Kushnir, and M.A. Cane, 2000: Reduced space optimal interpolation of historical marine sea level pressure. *J. Climate*, **13**, 2987–3002.
- Kistler, R., E. Kalnay, W. Collins, S. Saha, G. White, J. Woollen, M. Chelliah, W. Ebisuzaki, M. Kanamitsu, V. Kousky, H. van den Dool, R. Jenne, and M. Fiorino, 2001: The NCEP-NCAR 50-Year Reanalysis: Monthly Means CD-ROM and Documentation. *Bull. Amer. Meteor. Soc.*, **82**, 247–268.
- Kitoh, A., H. Koide, K. Kodera, S. Yukimoto, and A. Noda, 1996: Interannual variability in the stratospheric-tropospheric circulation in an ocean-atmosphere coupled GCM. *Geophys. Res. Lett.*, **23**, 543–546.
- Kitoh, A., S. Yukimoto, and A. Noda, 1999a: ENSO-monsoon relationship in the MRI coupled GCM. *J. Meteor. Soc. Japan*, **77**, 1221–1245.
- , T. Motoi, and H. Koide, 1999b: SST variability and its mechanism in a coupled atmosphere/mixed-layer ocean model. *J. Climate*, **12**, 1221–1239.

- Kodera, K., M. Chiba, H. Koide, A. Kitoh, and Y. Nikaidou, 1996: Interannual variability in the winter stratosphere and troposphere in the Northern Hemisphere. *J. Meteor. Soc. Japan*, **74**, 365–382.
- Kushner, P.J., I.M. Held, and T.L. Delworth, 2003: Southern Hemisphere Atmospheric Circulation Response to Global Warming. *J. Climate*, **14**, 2238–2249.
- Knutson, T.R. and S. Manabe, 1995: Time-mean response over the tropical Pacific to increased CO<sub>2</sub> in a coupled ocean-atmosphere model. *J. Climate*, **8**, 2181–2199.
- and ———, 1998: Model assessment of decadal variability and trends in the tropical Pacific Ocean. *J. Climate*, **11**, 2273–2296.
- Manabe, S. and R. Wetherald, 1967: Thermal equilibrium of the atmosphere with a given distribution of relative humidity. *J. Atmos. Sci.*, **24**, 241–259.
- , R.J. Stouffer, M.J. Spelman, and K. Bryan, 1991: Transient responses of a coupled ocean-atmosphere model to gradual changes of atmospheric CO<sub>2</sub>, Part I: Annual mean response. *Journal of Climate*, **4**, 785–818.
- Meehl, G.A. and W.M. Washington, 1996: El Niño-like climate change in a model with increased atmospheric CO<sub>2</sub> concentrations. *Nature*, **382**, 56–60.
- Murphy, J.M. and J.F.B. Mitchell, 1995: Transient response of the Hadley Centre coupled ocean-atmosphere model to increasing carbon dioxide. Part II: Spatial and temporal structure of response. *J. Climate*, **8**, 57–80.
- Noda, A., S. Nakagawa, T. Motoi, S. Yukimoto, and T. Tokioka, 1996: Global warming induced by CO<sub>2</sub> and the Okhotsk Sea. *J. Remote Sensing Soc. Japan*, **16**, 89–99.
- , K. Yoshimatsu, A. Kitoh, and H. Koide, 1999a: Relationship between natural variability and CO<sub>2</sub>-induced warming pattern: MRI coupled atmosphere/mixed-layer ocean (slab) GCM Experiment. Preprint Volume of the 10th Symposium on Global Change Studies, 10–15 January 1999, Dallas, Texas. 5A.1.
- , ———, S. Yukimoto, K. Yamaguchi, and S. Yamaki, 1999b: Relationship between natural variability and CO<sub>2</sub>-induced warming pattern: MRI AOGCM Experiment. Preprint Volume of the 10th Symposium on Global Change Studies, 10–15 January 1999, Dallas, Texas. 5A.2.
- , 2000: Global climate change projection due to global warming. *Tenki*, **47**, 702–708. (in Japanese)
- Palmer, T.N., 1993: A nonlinear dynamical perspective on climate change. *Weather*, **48**, 313–348.
- , 1999: Nonlinear dynamical perspective on climate prediction. *J. Climate*, **12**, 575–591.
- Perlwitz, J. and H.-F. Graf, 1995: The statistical connection between tropospheric and stratospheric circulation of the Northern Hemisphere in winter. *J. Climate*, **8**, 2281–2295.
- Reader, M.V. and G.J. Boer, 1998: The modification of greenhouse gas warming by the direct effect of sulphate aerosols. *Clim. Dyn.*, **14**, 593–607.
- Rind, D., P. Lonergan, N.K. Balachandran, and D. Shindell, 2002: 2 × CO<sub>2</sub> and solar variability influences on the troposphere through wave-mean flow interaction. *J. Meteor. Soc. Japan*, **80**, 863–876.
- Shindell, D.T., R.L. Miller, G.A. Schmidt, and L. Pandolfo, 1999: Simulation of recent northern winter climate trends by greenhouse gas forcing. *Nature*, **399**, 452–455.
- , G.A. Schmidt, R.L. Miller, and D. Rind, 2001: Northern hemisphere winter climate response to greenhouse gas, ozone, and volcanic forcing. *J. Geophys. Res.*, **106**, 7193–7210.
- Smith, T.M. and R.W. Reynolds, 2004: Improved Extended Reconstruction of SST (1854–1997). *J. Climate*, **17**, 2466–2477.
- Sugi, M., A. Noda, and N. Sato, 2002: Influence of the global warming on tropical cyclone climatology: An experiment with the JMA global model. *J. Meteor. Soc. Japan*, **80**, 249–272.
- and J. Yoshimura, 2004: A mechanism of tropical precipitation change due to CO<sub>2</sub> increase. *J. Climate*, **17**, 238–243.
- Takata, K. and A. Noda, 1997: The effect of cumulus convection on CO<sub>2</sub>-induced climate change. *J. Meteor. Soc. Japan*, **75**, 677–686.
- Tanaka, H.L., N. Ishizaki, and D. Nohara, 2005: Intercomparison of the intensities and trends of Hadley, Walker and monsoon circulations in the global warming projections. *SOLA*, **1**, 77–80, doi: 10.2151/sola.2005-021.
- Thompson, D.W. and J.M. Wallace, 1998: The Arctic Oscillation signature in the wintertime geopotential height and temperature fields. *Geophys. Res. Lett.*, **25**, 1297–1300.
- Timmermann, A., J. Oberhuber, A. Bacher, M. Esch, M. Latif, and E. Roeckner, 1999: Increased El Niño frequency in a climate model forced by future greenhouse warming. *Nature*, **398**, 694–696.
- Tokioka, T., A. Noda, A. Kitoh, Y. Nikaidou, S. Nakagawa, T. Motoi, S. Yukimoto, and K. Takata, 1995: Transient CO<sub>2</sub> experiment with the MRI CGCM—Quick report—. *J. Meteor. Soc. Japan*, **73**, 817–826.
- , ———, ———, ———, ———, ———, ———, and ———, 1996: Transient CO<sub>2</sub> experiment with the MRI CGCM—Annual mean

- response—. *CGER's Supercomputer Monograph Report Vol. 2*, National Institute for Environmental Studies, Tsukuba, Japan, 86pp.
- Trenberth, K.E. and D.A. Paolino, 1980: The Northern Hemisphere sea-level pressure data set: Trends, errors and discontinuities. *Mon. Wea. Rev.*, **108**, 855–872.
- Wetherald, R. and S. Manabe, 2002: Simulation of hydrologic changes associated with global warming. *J. Geophys. Res.*, **107**, D19, 4379, doi:10.1029/2001JD001195.
- Yamazaki, K. and Y. Shinya, 1999: Analysis of the Arctic Oscillation simulated by AGCM. *J. Meteor. Soc. Japan*, **77**, 1287–1298.